Journal of Electrical and Electronic Engineering
2025; 13(1): 24-39
http://www.sciencepublishinggroup.com/j/jeee
doi: 10.11648/j.jeee.20251301.13
ISSN: 2329-1613 (Print); ISSN: 2329-1605 (Online)

Nested Hexagonal Split Ring Resonator-Based Metamaterial for Performance Enhancement in Multiband Antenna

Hassan Belaid

National School of Applied Sciences (ENSATé), Abdelmalek Essaadi University, Tétouan, Morocco

Email address:
belaid.hassan@etu.uae.ac.ma (Hassan Belaid), belaidhassan201@gmail.com (Hassan Belaid)

To cite this article:
Hassan Belaid. (2025). Nested Hexagonal Split Ring Resonator-Based Metamaterial for Performance Enhancement in Multiband Antenna. *Journal of Electrical and Electronic Engineering, 13*(1), 24-39. https://doi.org/10.11648/j.jeee.20251301.13

Received: 17 December 2024; **Accepted:** 8 January 2025; **Published:** 6 February 2025

Abstract: In this paper, we present a Nested hexagonal shaped split-ring resonator based negative epsilon metamaterials layered on 11 $mm \times 10\ mm \times 1.524\ mm$ Rogers RO4350B dielectric substrate and designed to enhance the performance of multiband satellite antennas. Simulations using CST electromagnetic software show that the NH-SRR metamaterial manifests seven distinct resonance frequencies of S_{21} spectrum at 2.37, 3.92, 5.4, 7.71, 8.58, 9.73 and 10.94 GHz, spanning S, C, and X-bands. The unit cell yields an effective medium ratio (EMR) of 12.66 and an electrical dimension of $0.087\lambda \times 0.079\lambda$ when calculated at 2.37 GHz, which implies the effectiveness and compactness of the NH-SRR shaped metamaterial. The simulated outcomes also revealed that negative electric permittivity (ϵ) response is attained within 4.16-5.75 GHz, 10.16-11.58 GHz and 14.46-16 GHz, with Near-Zero permeability property near the resonance frequencies. Our methodology involves using multiple electromagnetic software tools, including CST, HFSS and COMSOL for simulation results and design validation. A detailed numerical analysis was conducted to assess the impact of using this metamaterial as array cover above a Log Periodic Dipole Array (LPDA) Antenna on the performance metrics, demonstrated that the LPDA with metamaterial superstrate surpasses the conventional antenna in term of gain, return in loss and impedance matching, particularly at frequencies where negative permittivity and near-zero permeability properties are observed. These findings suggest that the NH-SRR metamaterial offers compactness, efficiency and scalability for applications in modern wireless communication and network systems.

Keywords: COMSOL, CST, HFSS, Effective Medium Ratio (EMR), HFSS, Nested Hexagonal Shaped Resonators, Negative Epsilon Metamaterial, LPDA Antenna, Split Ring Resonator

1. Introduction

Metamaterials have emerged as a revolutionary class of materials and have garnered significant attention due to their unique electromagnetic properties not found in naturally occurring substances. Metamaterials are typically composed of artificial periodic arrangements of sub-wavelength resonant structures embedded in a dielectric matrix [1]. These composite materials are designed to manipulate the optical characteristics as electric permittivity (ϵ), magnetic permeability (μ) and refractive index (n) to become low or even negative at some frequencies. This exotic behavior results in a counter-intuitive phenomena and reversal of the electromagnetic emissions direction, including negative refraction [1], where waves bend in the opposite direction to that predicted by Snell's law, perfect absorption [2], invisibility cloaking [3], reversed Cerenkov radiations [4], inverse Doppler effect [5] and so on.

One of the key areas of focus in metamaterial research is the manipulation of effective properties such as electric permittivity (ϵ). The theoretical foundation of materials with negative permittivity, also known as epsilon-negative (ENG) metamaterials is grounded in Maxwell's equations and Drude-Lorentz dispersion model, which describe the behavior of electromagnetic field interacting with materials with negative properties [6]. According to Drude model, the electric permittivity of a material is determined by the collective oscillation of free electrons in response to an external electromagnetic field. At frequencies below the plasma frequency, the electrons can no longer follow the oscillating field effectively, resulting in the displacement current and

the electric field to be out of phase. The ability to control permittivity enables the design of metamaterials that can support resonance at specific frequencies, leading to enhanced electromagnetic response and improved device performance. In fact, ENG metamaterials have been shown to enhance the performance of devices such as antennas and sensors [7, 8], critical components in modern wireless systems such as satellite communication, 5G, and ultra-wideband radar. In recent years, the demand for multi-band operational negative epsilon metamaterials has increased substantially because of the rapid growth of wireless communication applications [9]. Antennas are the main components in communication systems, and their performance is often limited by factors such as gain, bandwidth, and efficiency. Integrating negative epsilon metamaterials into antenna structures has shown promise in addressing these limitations. For example, Islam et al. introduced a compact $8\ mm \times 8\ mm$ square-enclosed circle SRR-based metamaterial [10], printed on a Rogers RO4350B substrate, achieving triple resonance bands at 2.61, 6.32, and 9.29 GHz with an effective medium ratio (EMR) of 14.37. The metamaterial exhibited negative permittivity and near-zero index properties and was used as an array cover to increase the horizontal gain of an LPDA antenna. Similarly, a tuned modified SRR quad-band metamaterial was employed in [11], and exhibited resonances at 2.38, 4.24, 5.98, 9.55, 12.1, and 14.34 GHz, with near-zero refractive index (NZI) characteristics and an EMR of 15.75. The metamaterial was used as a superstate array to improve the gain of an LPDA antenna. Additionally, Saravanan et al. reported on a phi-shaped slotted metamaterial that achieved simultaneous negative permittivity and permeability at 2.4 GHz and and is incorporated with a conventional patch antenna to improve gain performance [12], reduce the reflection coefficient, and maintain good radiation characteristics. Researchers in [13] studied a symmetric resonator based metamaterial, which displayed an EMR of 7.33 at 4.2 GHz, with four resonance modes at 4.20, 10.14, 13.15, and 17.1 GHz covering C, X and Ku bands. The metamaterial proposed for wireless multiband applications, achieved a negative epsilon and near zero permeability and refractive index properties. The authors in [14] deigned coupled ring resonator (CR-SRR) metamaterial that have multi-frequency resonances and a higher value of the effective medium ratio of 16.74. The proposed $8\ mm \times 8\ mm$ metamaterial unit cell exhibit negative permittivity at frequencies ranging from 2.15 to 2.3 GHz, 4.4-4.95 GHz, 5.7-6.1 GHz, 8.46-9.2 GHz, and 10.6-10.98 GHz, along with near-zero refractive indexes in the vicinity of these frequency ranges, which make the structure practical for wireless communications in S, C, X-bands. A research article made by Ajewole, Kumar, and Afullo on an I-shaped square metamaterial demonstrated resonant frequencies at 6.31, 7.79, 9.98, 10.82, 11.86, 13.36, and 15.5 GHz within the C, X, and K-bands, with an EMR of 4.75 and a negative permittivity response over multiple bands [15]. The proposed I-shaped resonator, printed on a low-cost FR-4 substrate and proposed for multi-band satellite communication systems, sub-6 GHz 5G applications, etc. In another investigation, Lima et al. explored the integration of a double negative metamaterial cells array into a microstrip patch antenna design in C-band applications with EMR of 11.75 [16]. The metamaterial proposed in their research showcased significant effectiveness in signal enhancement at 5.8 GHz where the capacitive loaded loop metamaterial is resonant. In a similar vein, Moniruzzaman et al. explored a $10\ mm \times 10\ mm$ cross-coupled interlinked SRR metamaterial with a maximum EMR of 8.03 [17], showing negative permittivity response across 3.95-5.65 GHz, 9.57-11.46 GHz, and 13.68-16 GHz, proposed for multiband satellite and radar communication applications. Furthermore, the authors in [18] proposed a novel dual-band metamaterial designed for S and C bands, providing wideband negative refractive index sensing and achieving an EMR of 6.93 at 2.7 GHz. This structure was fabricated on a $16\ mm \times 16\ mm \times 1.6\ mm$ FR-4 substrate and designed for use in advanced satellite communications systems. A square-shaped SRR metamaterial absorber printed on $9.5\ mm \times 9.5\ mm \times 1.6\ mm$ FR-4 substrate and designed for sub-6 GHz applications, was presented in [19]. It demonstrated a 90% absorption peak at 2.5 GHz, 4.9 GHz, and 6 GHz, with a maximum EMR of 9.96. The proposed metamaterial absorber also exhibited single-negative metamaterial properties, making it practical for use in specific frequency bands of 5G applications such as signal absorption, crowd sensing, SAR reduction, etc. In [20], Alam et al. developed a compact $0.51\lambda \times 0.51\lambda$ metamaterial-based antenna fabricated on Rogers 5880 substrate material, designed for Ku-band nano-satellite communication systems. The antenna achieved circular polarization with a realized gain of 6.69 dB. Lastly, Hossen et al. studied a $14.5\ mm \times 14.5\ mm$ square-shaped SRR metamaterial that exhibited an EMR of 6.2, with resonances at 4.3 GHz and 9.1 GHz, making it applicable for wireless applications [21].

Given the advantageous electromagnetic featured epsilon-negative metamaterials and their demonstrated benefits in enhancing antenna performance, this study aims to analyze a novel nested hexagonal-shaped split-ring resonator (NH-SRR) metamaterial, designed to operate across the S, C, and X bands, with a focus on enhancing gain, reducing radiation loss, and achieving compactness for advanced wireless communication systems, including satellite and 5G networks.

2. Method and Simulation

2.1. Configuration of the NH-SRR Metamaterial Unit Cell

The three-dimensional schematic view of the Nested Hexagonal split-ring resonator (NH-SRR) unit cell arrangement is depicted in Figure 1. The hexagonal shape of the resonators was chosen due to the high capacitive loading this structure creates, which enhances its resonance behavior. Its broadside geometry effectively minimizes bi-anisotropic responses and mitigates cross-polarization effects within the dielectric medium. This characteristic is particularly

advantageous for applications requiring minimal interference. The design geometry of the resonators comprises four nested hexagons, each progressively smaller by a scaling factor of 0.8 to ensure multiple resonant frequencies. The largest hexagon has a length of 8.66 mm and the smallest is about $4.43\ mm$. Each ring has a width of $w = 0.2\ mm$ and features gap splits introduced in the front, displaced by $180°$ with a gab width of $g = 0.2\ mm$. The resonators patch are made of annealed copper metal with a thickness of 0.035 mm and conductivity of $\sigma = 5.8 \times 10^7\ S/m$. The dielectric substrate is Rogers RO4350B with a thickness, relative permittivity and loss tangent are $1.524\ mm$, $\epsilon_r = 3.66$ and $tan\delta = 0.0031$, respectively. The unit cell of the metamaterial has a physical size of $11\ mm \times 10\ mm$. The optimized dimension parameters of the NH-SRR based metamaterial unit cell are listed in Table 1. The full-wave finite integration technique (FIT) based on high-frequency electromagnetic solver in the computer simulation technology microwave studio (CST MWS) was used to carry out the numerical analysis and optimization of the design geometry. Two waveguide ports were applied and placed along the Z-axis: the first port acts as the transmitting port for the reflecting signal, while the second port serves as the receiving port. A transverse electromagnetic signal is incident vertically on the SRR patch surface from one waveguide port to energize the metamaterial sample. The X-axis and Y-axis were assigned to perfect electric and magnetic boundary conditions, respectively. The operating frequency in this study was set between 2-12 GHz, ensuring the homogenization requirements of the effective medium.

Table 1. *Geometrical parameters value of the designed metamaterial.*

Parameter	A1	A2	L1	L2	L3	L4	w	g
Value (mm)	11	10	8.66	6.93	5.54	4.43	0.35	0.2

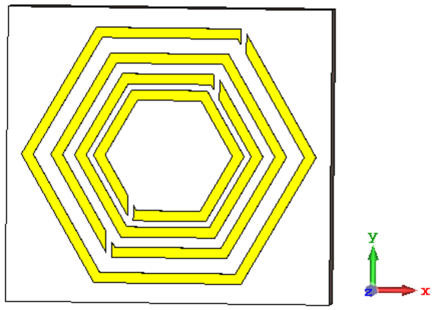

Figure 1. *Front view of the Nested Hexagonal Split ring resonator metamaterial.*

2.2. Optical Properties Extraction Method

The effective electromagnetic characterization of the reported metamaterial, including electric permittivity $\epsilon(\omega)$, magnetic permeability $\mu(\omega)$, refractive index n(ω), and impedance $z(\omega)$, are determined based on the complex S-parameters obtained from the simulation using the well known Robust technique [22]. To achieve this, a MATLAB script was employed, incorporating the Robust method equations to accurately determine the effective electromagnetic properties of the metamaterial sample. The extraction process utilizes the following formulas [23, 24]:

$$S_{11} = \left(\frac{R_{01}(1 - e^{i2nk_0d})}{1 - R_{01}^2 e^{i2nk_0d}} \right) \tag{1}$$

$$S_{21} = \left(\frac{(1 - R_{01}^2)e^{i2nk_0d}}{1 - R_{01}^2 e^{i2nk_0d}} \right) \tag{2}$$

Where k_0 is the wave vector in free space, d is the thickness of the dielectric substrate and R_{01} is the ratio expressed by:

$$R_{01} = \frac{Z(\omega) - 1}{Z(\omega) + 1} \tag{3}$$

$$Z(\omega) = \pm \sqrt{\frac{(1 + S_{11}^2) - S_{21}^2}{(1 - S_{11}^2) - S_{21}^2}} \tag{4}$$

$$e^{2ink_0d}(\omega) = \frac{S_{21}}{1 - S_{11}\frac{Z(\omega)-1}{Z(\omega)+1}} \tag{5}$$

The refraction index is calculated using the relation:

$$n(\omega) = \frac{1}{k_0 d} \left[\left\{ imag(\ln(e^{2ink_0d})) + 2m\pi \right\} - i \left\{ real(\ln(e^{2ink_0d})) \right\} \right] \tag{6}$$

The permittivity is determined by the relation:

$$\epsilon(\omega) = \frac{n(\omega)}{Z(\omega)} \tag{7}$$

and the permeability $\mu(\omega)$

$$\mu(\omega) = n(\omega).Z(\omega) \tag{8}$$

3. Results and Discussion

3.1. Scattering and Effective Medium Parameters of NH-SRR Metamaterial

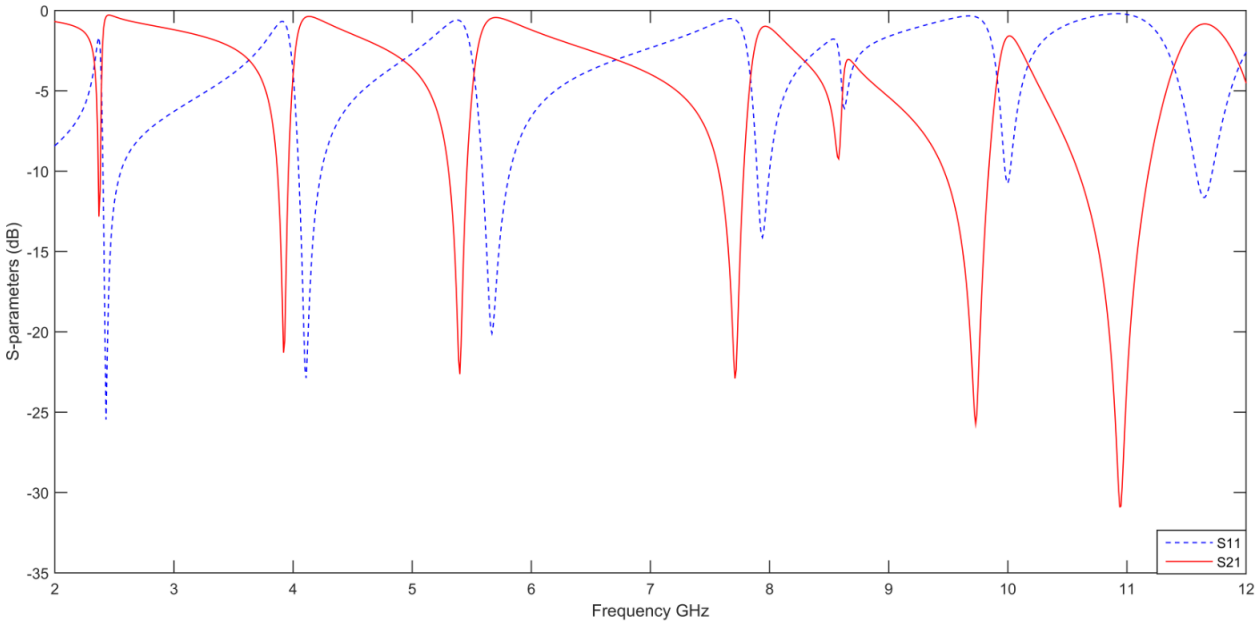

Figure 2. *S-parameters of the Nested Hexagonal SRR metamaterial.*

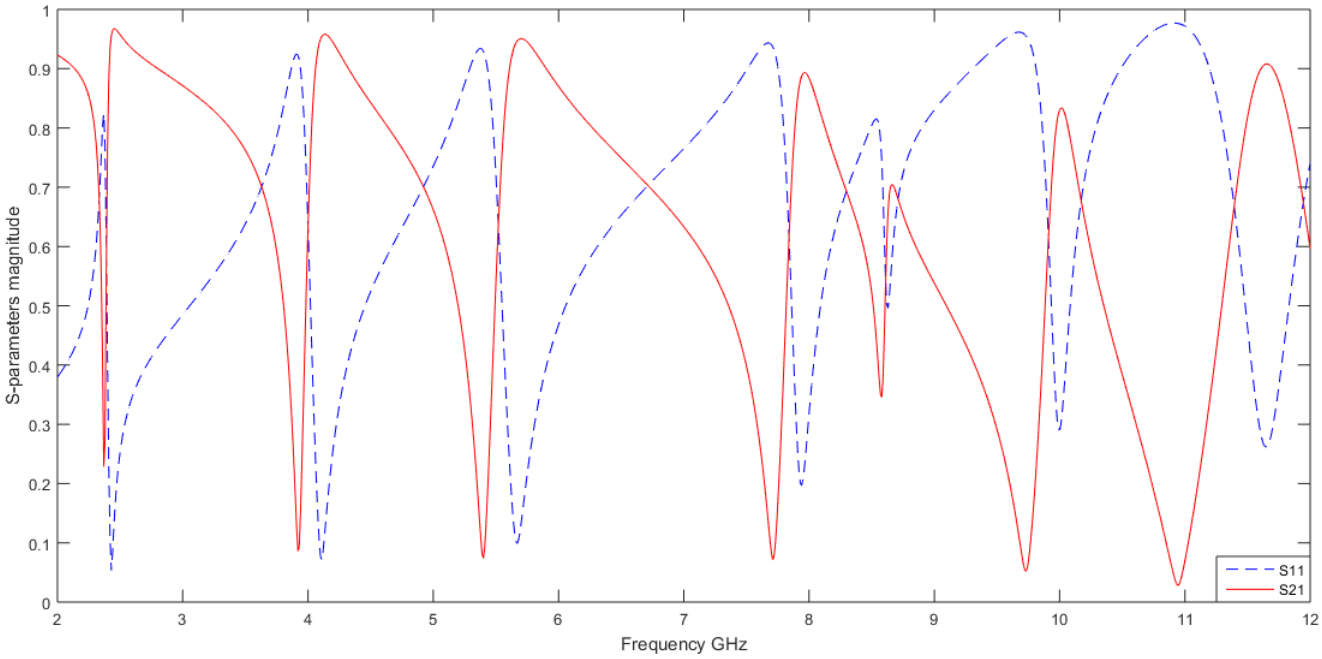

(a) Magnitude

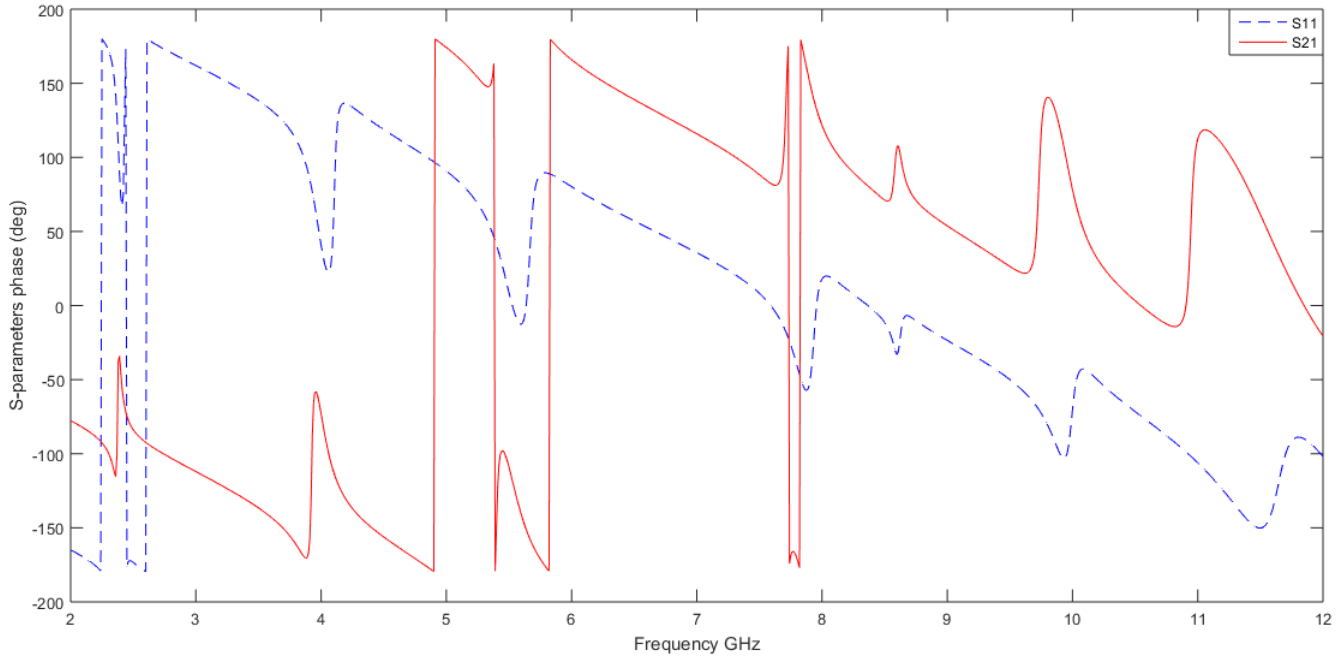

(b) Phase

Figure 3. *The variation of the S-parameters in function of frequency in the term of (a) magnitude (b) phase.*

In this section, simulation results of the Nested Hexagonal shaped SRR compact metamaterial are presented. For the scattering parameters of the CST simulation output plotted in Figure 2, the S_{21} findings of the unit cell within the 2-12 GHz range revealed a total of seven distinct resonance frequency peaks located at 2.37 GHz, 3.92 GHz, 5.4 GHz, 7.71 GHz, 8.58 GHz, 9.73 GHz and 10.94 GHz with a return in loss of -12.83 dB, -21.3 dB, -22.63 dB, -22.9 dB, -9.23 dB, -25.73 dB and -30.91 dB, respectively. These seven findings of resonance frequencies lies within the microwave region, namely 1-2 GHz, 4-6 GHz, and 14-16 GHz, which depict the S, C and X band. The bandwidth of S_{21} using less than -10 dB is 0.02 GHz (2.36-2.38 GHz), 0.09 GHz (3.87-3.96 GHz), 0.15 GHz (5.31-5.46 GHz), 0.2 GHz (7.58-7.78 GHz), 0.34 GHz (9.5-9.84 GHz) and 0.55 GHz (10.62-11.17 GHz). On the other hand the reflection coefficient S_{11} (blue curve) displays dips at 2.43 GHz, 4.11 GHz, 5.67 GHz, 7.94 GHz, 8.63 GHz, 9.99 GHz and 11.66 GHz with exposed magnitudes of -25.46 dB, -22.88 dB, -20.09 dB, -14.12 dB, -6.09 dB, -10.67 dB and -11.58 dB, accordingly. It was observed from the same figure that when the S_{11} magnitude is minimum, then the transmittance at that resonant frequency is maximum. Given that the frequency of every S_{21} minimum is always lower than the corresponding S_{11} minimum frequency, each observed resonance can be attributed to electrical resonance within the resonators structure. The unit cell maximum EMR value of 12.66 when calculated at 2.37 GHz improves its homogeneity and reduces its compact electrical size, which is of $0.087\lambda \times 0.079\lambda$. The phase and magnitude plots of the scattering parameters are presented in Figure 3b and Figure 3a, which demonstrates that the input wave with the output of reflected and transmitted varies in $-\pi$ to $+\pi$ with the total phase change is 2π. As the frequency approaches a resonance peak, the phase of S_{11} undergoes a sharp transition, typically shifting by nearly 180 degrees. This phase shift is characteristic of resonance behavior which is an indicative of a change and reduction in the direction of the reflected power at these frequencies. The phase of S_{21} also undergoes sharp variations around these resonance points due to dispersion. Furthermore, the magnitude of S_{21} shows significant dips which implies a reduction in transmitted power because of the strong reflection around these specific frequencies. From Figure 4a it can be observed that the NH-SRR metamaterial produces negative effective permittivity responses in the S-band and C-band for the frequency ranges 2.36-2.4, 3.6-3.98, 4.51-5.42 and 5.81-6.18 GHz. Additionally, it was noticed that the permittivity undergoes a transition from positive and maximum value to negative minimum value when resonance occurs in 2.37 GHz with a maximum peak magnitude of -26.39. This behavior aligns with the Drude-Lorentz dispersion model and can be explained by [6]:

$$\epsilon(\omega) = 1 + \frac{\omega_p^2}{\omega_0^2 - \omega^2 - i\omega\gamma} \tag{9}$$

where γ denote the damping factor that represents the dissipation of energy into system, and ω_0 is the resonance frequency respectively. Negative permittivity originates from the collective oscillations of free electrons or other polarizable entities within the metal when exposed to an external electromagnetic field. As the frequency of the incident wave approaches regions below a critical frequency, typically the plasmon frequency (ω_p), these oscillations occur out of phase with the driving field, resulting in an effective phase

opposition and thus a negative real part of permittivity. A close investigation of the magnetic permeability (μ) graph against frequency, shown in Figure 4b, reveals that the real part of is observed to be negative in the C and X bands, specifically at 7.62-7.85 GHz, 9.05-9.84 GHz, and 10.23-11.1 GHz, with nearly equal to zero values seen at the frequency bands where metamaterial shows epsilon negative characteristics. The nearly equal to zero values of the real part of normalized impedance (z) in Figure 4c, seen at each resonance peak further highlight the passive nature of the proposed metamaterial. Given that the effective permittivity of the unit cell becomes negative within specific frequency ranges, this material can be classified as epsilon negative metamaterial (ENG). This feature allows the NH-SRR based metamaterial to be applicable for a wide range of electromagnetic purposes in communication sector such as for bandwidth, gain and directivity enhancement of antenna, radars and other telecommunication systems.

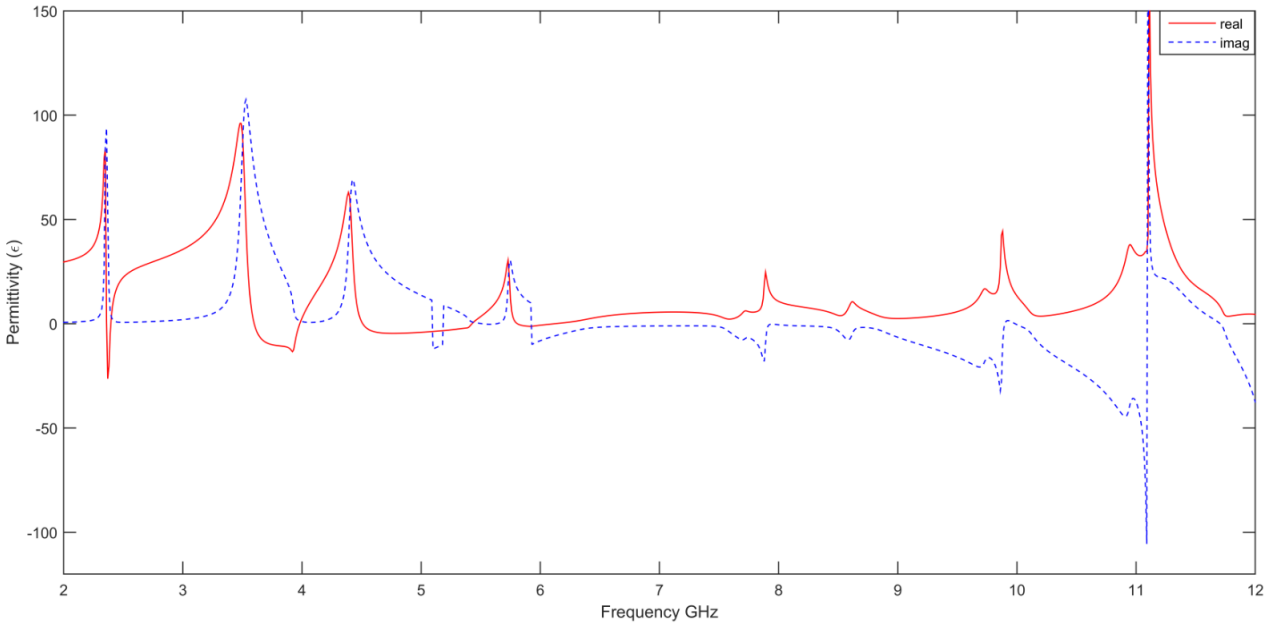

(a) Electric permittivity $\epsilon(\omega)$

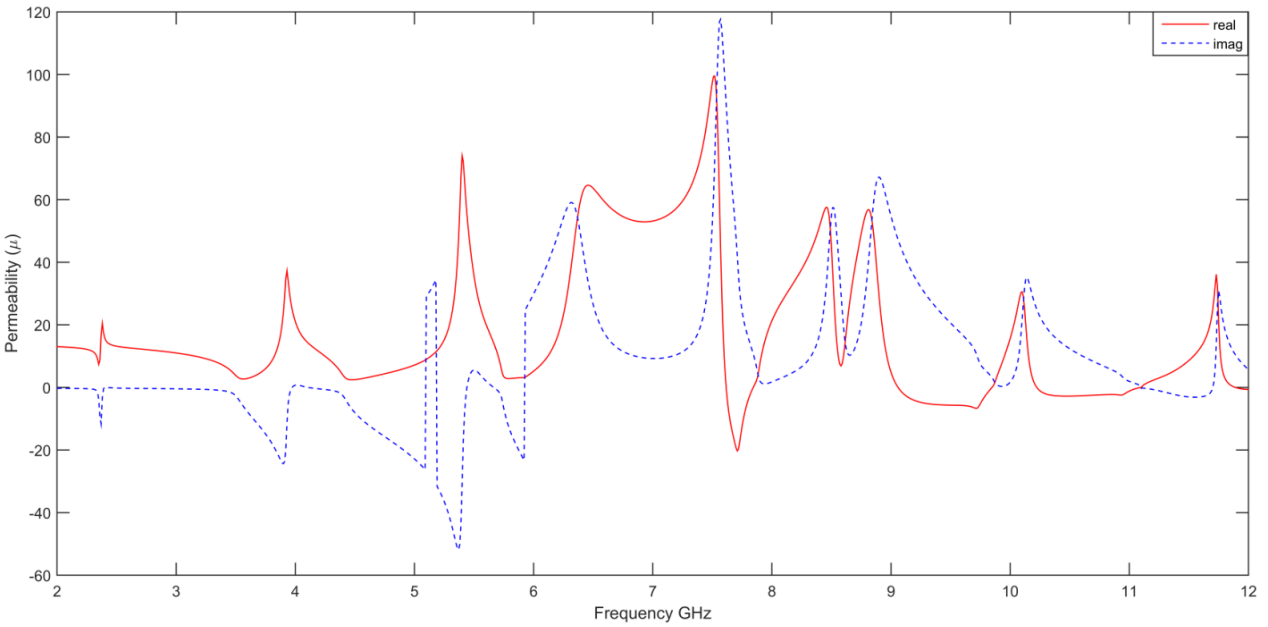

(b) Magnetic permeability $\mu(\omega)$

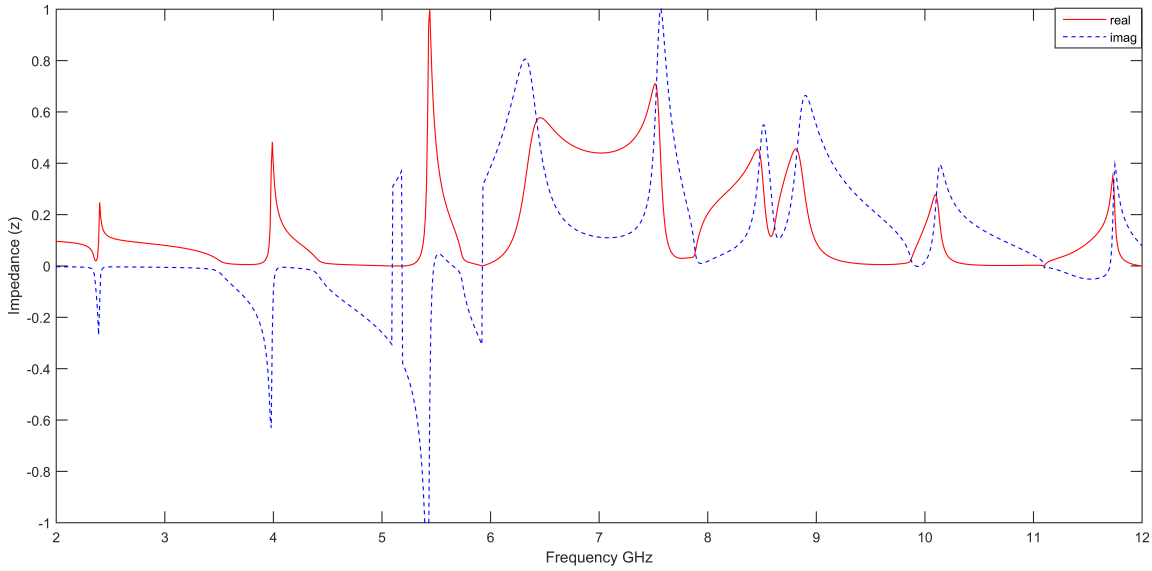

(c) Refraction index n(ω)

Figure 4. *The effective optical properties of the Nested Hexagonal Square resonator metamaterial as function of frequency.*

3.2. Validation of Simulation Results

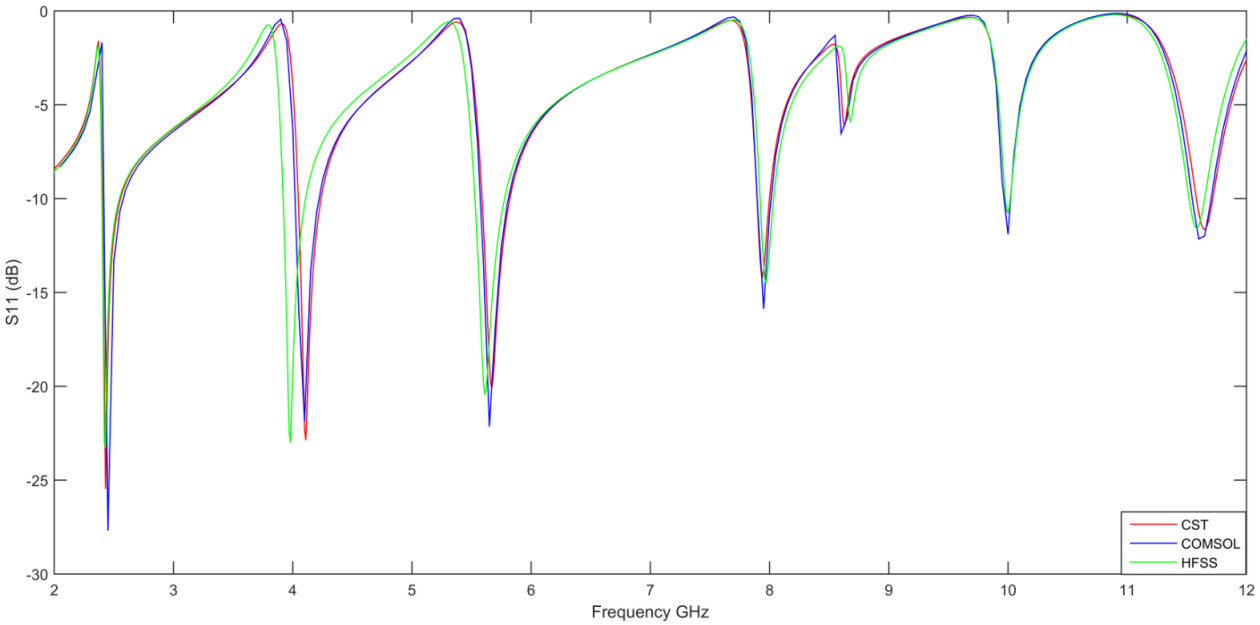

(a) Reflection (S_{11})

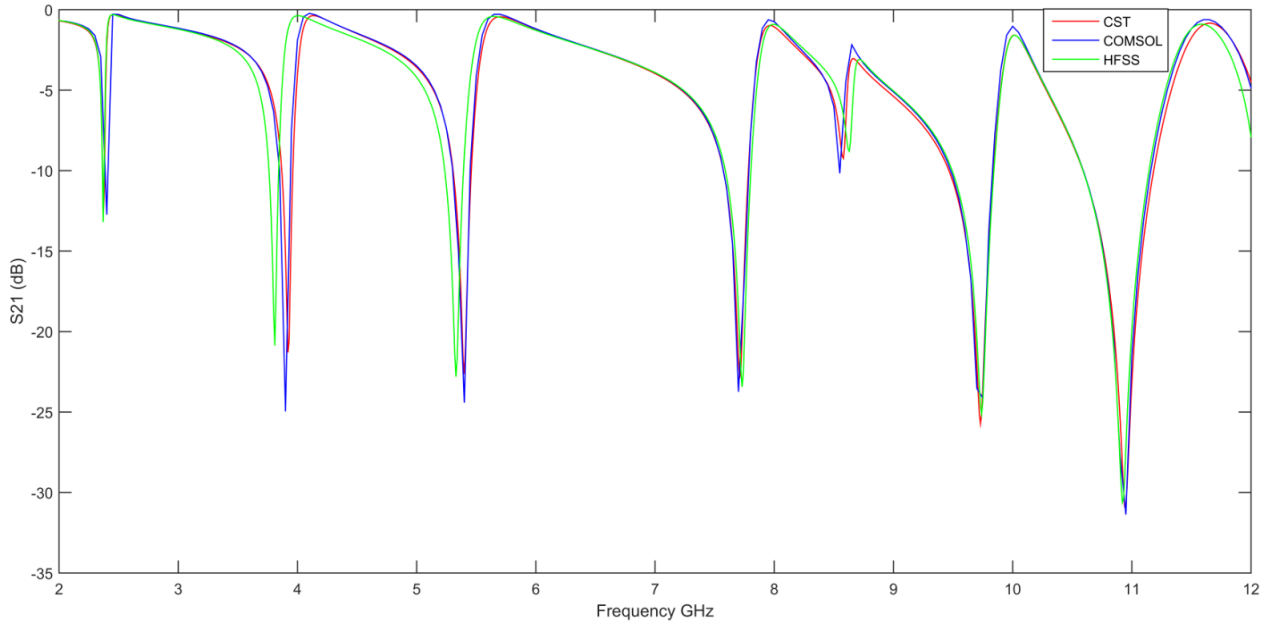

(b) Transmission (S_{21})

Figure 5. *S-parameters data results across all simulation platforms.*

A comparative analysis was performed using CST Microwave Studio, COMSOL Multiphysics, and Ansys HFSS to cross verify the electromagnetic performance of the nested hexagonal split-ring resonator (NH-SRR) metamaterial design. From Figure 5a and Figure 5b it is evident that all three software platforms were consistent in identifying the seven distinct resonant frequencies and their corresponding magnitudes, with roughly the same bandwidth for both coefficients. In the HFSS simulation, the transmittance exhibited resonant frequencies at 2.37 GHz, 3.81 GHz, 5.33 GHz, 7.73 GHz, 8.63 GHz, 9.74 GHz, and 10.92 GHz, with corresponding gains of -13.2 dB, -20.87 dB, -22.81 dB, -23.43 dB, -8.79 dB, -25.13 dB, and -30.62 dB, respectively. The reflection coefficient showed resonance peaks at 2.43 GHz, 3.98 GHz, 5.61 GHz, 7.97 GHz, 8.68 GHz, 10 GHz, and 11.58 GHz, with amplitudes of -23.21 dB, -22.99 dB, -20.38 dB, -14.47 dB, -5.98 dB, -10.75 dB, and -11.58 dB, respectively. In terms of COMSOL simulation outputs, resonance frequencies of S_{21} parameter were observed at 2.4 GHz, 3.9 GHz, 5.4 GHz, 7.7 GHz, 8.55 GHz, 9.75 GHz, and 10.75 GHz, with gains of -12.73 dB, -24.96 dB, -24.41 dB, -23.74 dB, -10.17 dB, -24.12 dB, and -37.35 dB, respectively. While, the peaks of the reflection coefficient S_{11} are located at 2.45 GHz, 4.1 GHz, 5.56 GHz, 7.95 GHz, 8.6 GHz, 10 GHz, and 11.6 GHz, with magnitudes of -27.69 dB, -21.88 dB, -22.15 dB, -15.9 dB, -6.6 dB, -12 dB, and -12.18 dB, accordingly. Therefore, the results indicate only minor discrepancies of a few MHz between the simulation tools, due to each software's unique computational approach and are within acceptable ranges for practical applications. Overall, this alignment across platforms validates the design's robustness and confirms the accuracy of the simulated electromagnetic response, demonstrating that the NH-SRR metamaterial's resonance behavior is both reliable and replicable.

3.3. Parametric Analysis

In this section, several comprehensive studies were conducted to investigate the impact of various key parameters on the resonant frequencies and overall electromagnetic performance of the nested hexagonal split-ring resonator (NH-SRR) design. Through systematic variation and simulation of these parameters, optimized and extraordinary performance trade-offs can be gained in relevance to the proposed satellite applications within the simulated frequency band.

3.3.1. Substrate Material

A detailed parametric study was conducted to examine how varying the substrate material impacts the resulting electromagnetic behavior and the performance of the nested hexagonal split-ring resonator (NH-SRR) design. The study involved selecting four Rogers dielectric materials, such as RO4003C, RO4350B, RT5870 and RT5880. Figure 6 shows that RO4350B and RO4003C exhibited seven resonance frequencies, while RT5870 and RT5880 showed six. RO4003C displayed a more consistent return loss but had a slightly lower maximum EMR (12.48) compared to RO4350B (12.66) at 2.37 GHz. Substrates with higher relative permittivity shifted resonant frequencies to lower values due to increased effective capacitance, while lower permittivity resulted in higher frequencies. Additionally, substrates with lower loss tangents (RT5880, RT5870) produced sharper resonance peaks, whereas higher loss tangents (RO4003C) led to broader, less distinct resonances due to increased dielectric losses as seen in Table 2. Ultimately, Rogers RO4350B was identified as the optimal substrate material for the proposed structure due to its higher EMR value and its ability to cover the desired frequency bands.

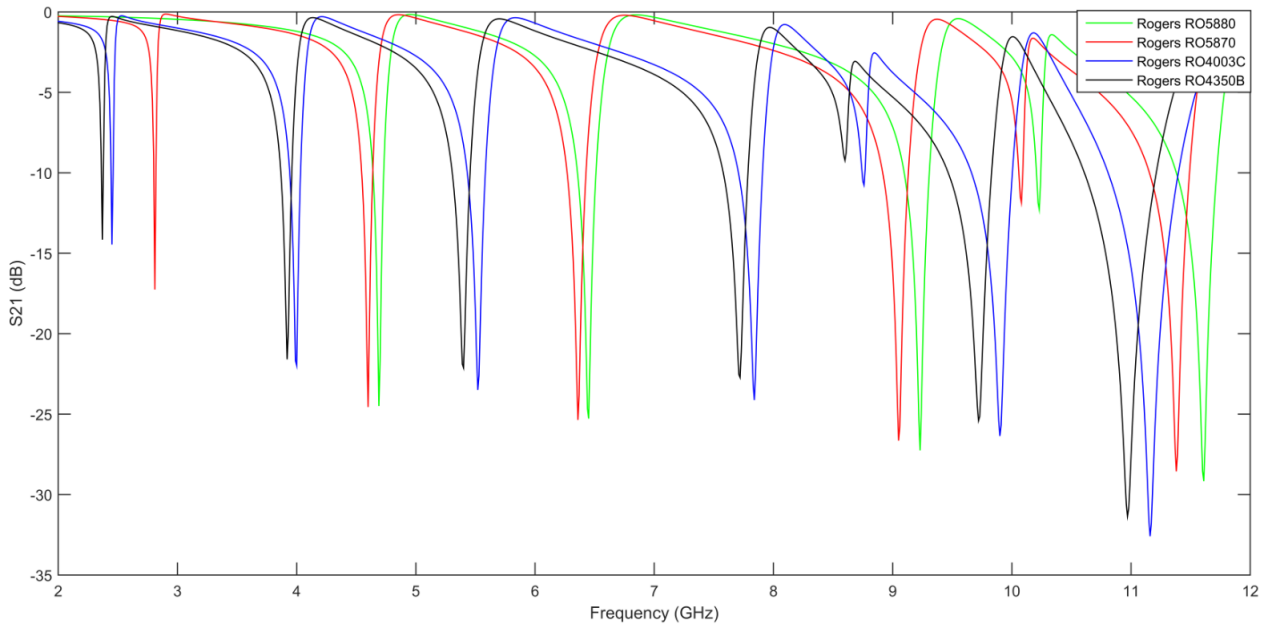

Figure 6. *Simulated S_{21} parameter of the Nested Hexagonal SRR on different substrates.*

Table 2. *Transmission overall outcomes for the different substrate materials.*

Substrate	ϵ_r	Loss Tangent (γ)	Thickness (mm)	Resonance frequency (f_0)	Covering band	Max EMR
RT5880	2.2	0.0009	1.575	2.88;4.7;6.45;9.23;10.21;11.61	S and X	10.41
RT5870	2.33	0.0012	1.57	2.81;4.6;6.36;9.05;10.08;11.39	S, C and X	12.87
RO4003C	3.55	0.0027	1.524	2.44;3.99;5.5;7.81;9.87;11.12	S, C and X	8.45
RT4350B	3.66	0.0037	1.524	2.37;3.92;5.4;7.71;8.58;9.73;10.94	S, C and X	12.66

3.3.2. Resonator Rotation

In this analysis, the adopted Nested Hexagonal metamaterial design was rotated anticlockwise by $90°$ angle each cycle. The observation of S-parameters curves in Figure 7 reveals noticeable changes that occurred in the electromagnetic performance as a result of the rotation. Specifically, the designs rotated by $90°$ and $270°$ manifested lower frequencies for the 4th and 5th resonance peaks compared to the $180°$ and initial design. Its noteworthy that the rotation angle of $90°$ and $270°$ showed similar responses, while both $180°$ and the initial design also demonstrated comparable behavior because the designed resonator structure is symmetrical. After further examination, the $0/360°$ design was assigned as the final structure due to its consistent performance across the desired frequency bands.

Table 3. *The values of analyzed metamaterial sample transmission performance for the different SRR rotation arrangement.*

Rotation angle	Resonance frequency (f_0)	Magnitude (dB)	Max EMR
0 / 360 °	2.37;3.92;5.4;7.71;8.58;9.73;10.94	-12.83;-21.3;-22.63;-22.9;-9.23;-25.73;-30.91	12.66
90 °	2.37;3.93;5.41;7.43;9.62;10.99	-8.2;-15.65;-17.93;-31.7;-29.2;-20.3;-20.42	12.66
180 °	2.39;3.94;5.41;7.73;9.74;11.01	-14.55;-21.97;-22.6;-22.86;-25.44;-37.16	12.55
270 °	2.37;3.93;5.42;7.43;9.6;10.98	-8.2;-15.77;-17.6;-31.76;-29.35;-20.42	12.66

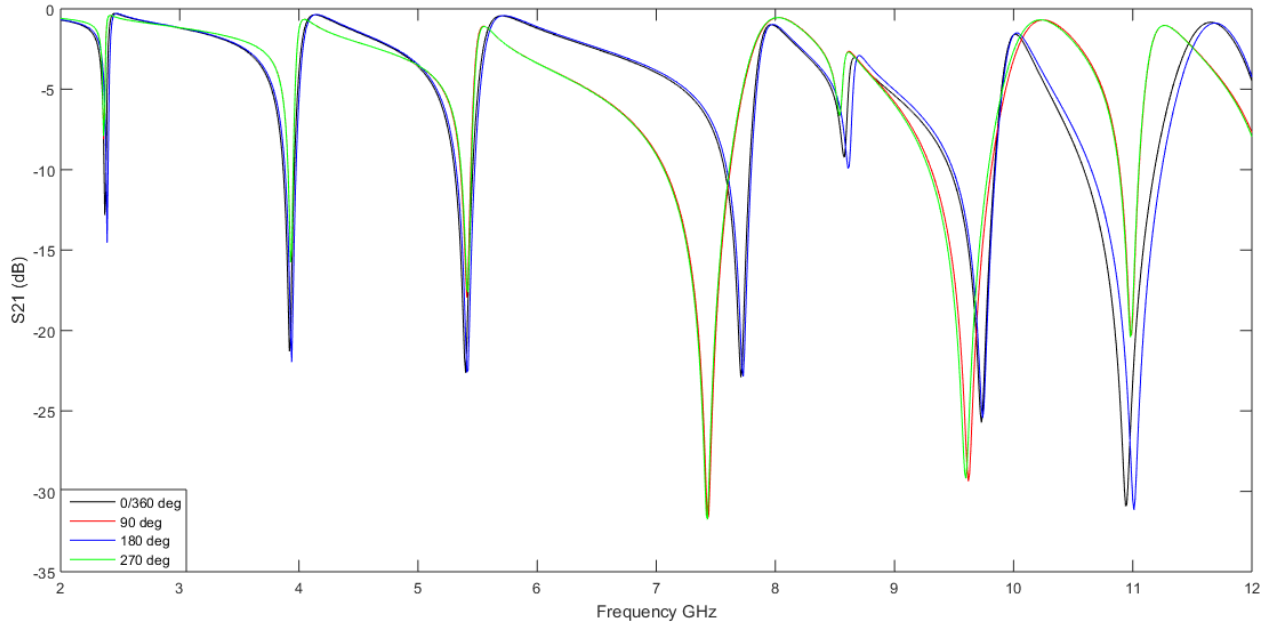

Figure 7. *Impact of rotating the resonators on S_{21} parameter.*

3.3.3. Split Gap Width

Various split gap widths (0.2 mm, 0.3 mm, 0.4 mm, and 0.5 mm) of the NH-SRR patch resonator were modified and analyzed to determine the optimal dimension for the proposed metamaterial. As shown in Figure 8, and Table 4, narrower gap widths generally resulted in higher resonant frequencies due to enhanced capacitive coupling, while wider gaps led to lower resonant frequencies. A noticeable shift in resonance frequency towards lower values was observed as the split gap decreased. This is because the capacitance (C) increases with a decrease in the split gap, and the resonance frequency is inversely proportional to the capacitance, as described by the relation.

$$f = \frac{1}{2\pi\sqrt{L.C}} \tag{10}$$

Superior performance characterized by a high value of EMR of 12.66 and well-separated resonances within the simulated frequency band, was achieved with gap width of 0.2 mm. Accordingly, the 0.2 mm gap width in the suggested structure is considered in this research.

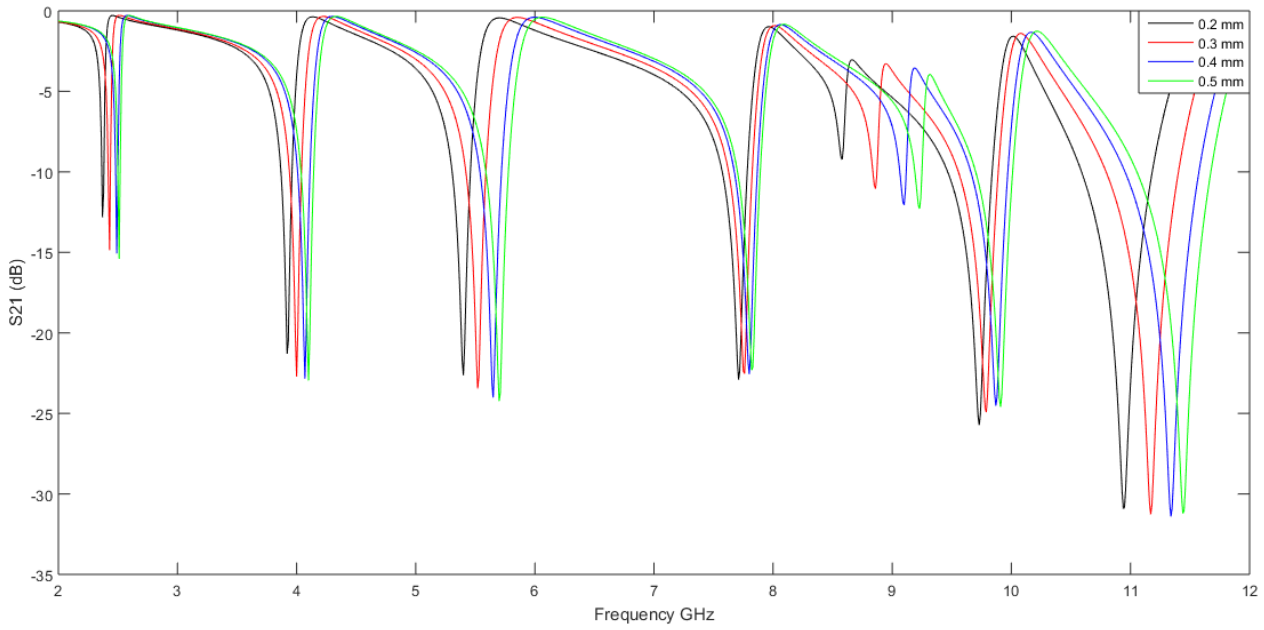

Figure 8. *Impact of changing the split gap on S_{21} parameter.*

Table 4. *The values of analyzed metamaterial sample transmission performance for the different split gaps width.*

Gap width	Resonance frequency (f_0)	Magnitude (dB)	Max EMR
0.2 mm	2.37; 3.92; 5.4; 7.71; 8.58; 9.73; 10.94	-12.83; -21.3; -22.63; -22.9; -9.23; -25.73; -30.91	12.66
0.3 mm	2.43; 4; 5.52; 7.76; 8.86; 9.79; 11.17	-14.87; -22.72; -23.45; -22.54; -10.85; -24.92; -31.27	12.34
0.4 mm	2.49; 4.07; 5.56; 7.8; 9.1; 9.87; 11.34	- 15.07; -22.84; -24.02; -22.56; -12.05; -24.52; -31.4	12.04
0.5 mm	2.51; 4.1; 5.7; 7.83; 9.23; 9.91; 11.45	-15.4; -22.96; -24.23; -22.13; -12.29; -24.6; -31.04	11.95

3.3.4. Resonators Width

Four resonator widths were evaluated to assess their impact on the overall electromagnetic properties, ranging from 0.25 mm to 0.55 mm in steps of 0.1 mm. Simulations were conducted for each width, with the resulting reflection and transmission curves presented in Figure 9. As shown in Table 5, wider resonators tend to slightly lower the resonant frequencies due to increased inductance, leading to sharper resonance peaks. This behavior is attributed to the increase in inductance (L) with greater resonator width, which in turn reduces the resonance frequencies. Although the 0.45 mm resonator width achieved the highest EMR at 2.24 GHz, it exhibited only six resonance peaks, similar to the 0.55 mm case, both having one fewer resonance frequency compared to the other widths. The optimal resonator width, which provided high EMR and seven resonance modes was found to be 0.35 mm. Consequently, a resonator width of 0.35 mm is selected for the recommended design.

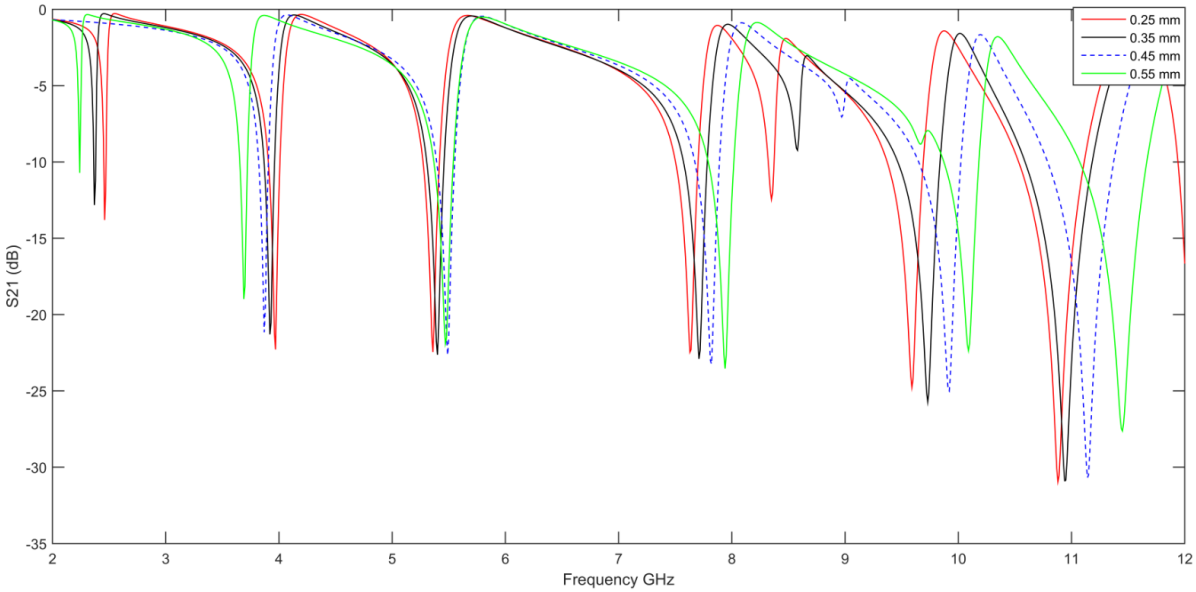

Figure 9. *Transmission graphs for the variation in resonator width.*

Table 5. *S_{21} results for the widths variation of the resonators.*

Strip width	Resonance frequency (f_0)	Magnitude (dB)	Max EMR
0.25 mm	2.46;3.97;5.36;7.63;8.35;9.59;10.88	-13.8;-22.29;-22.45;-22.47;-12.46;-24.78;-30.96	12.19
0.35 mm	2.37;3.92;5.4;7.71;8.58;9.73;10.94	-12.83;-21.3;-22.63;-22.9;-9.23;-25.73;-30.91	12.66
0.45 mm	3.87;5.49;7.82;8.97;9.92;11.14	-21.16;-22.56;-23.25;-7.05;-25.01;-30.69	7.75
0.55 mm	2.24;3.69;5.47;7.94;10.1;11.45	-10.72;-18.98;-21.89;-23.54;-21.91;-27.63	13.39

3.4. Study Comparison

The Effective Medium Ratio (EMR) is a key metric for assessing the utility and compactness of metamaterials, as it reflects the material's electromagnetic performance. EMR is defined as the ratio of wavelength λ_0 (at the lowest resonance frequency) to the unit cell dimension L:

$$EMR = \frac{\lambda_0}{L} \tag{11}$$

An EMR greater than 4 is required to maintain the material's subwavelength characteristics and effective homogeneity [10]. A high EMR ensures compliance with metamaterial design

standards and preserves desired optical properties [25, 26]. In our study, the NH-SRR-based metamaterial exhibits maximum EMR of 12.66 at 2.37 GHz, which demonstrates the unit cell's compactness, satisfying the $\lambda/10$ criterion with a size of 10 mm. This high EMR enhances homogeneity and reduces the electrical size to $0.087\lambda \times 0.079\lambda$, without compromising fabrication limits. A comparison has been accomplished between the proposed unit cell and other states of arts based on the electrical and physical dimension, resonance frequency, EMR and frequency bands of application as stated in Table 6, and several observations can be made. Firstly, the compact size of the proposed metamaterial ($11\ mm \times 10\ mm$) is comparable to other designs, such as the $8\ mm \times 8\ mm$ resonator introduced in [30], and the $9\ mm \times 9\ mm$ Circle-shaped SRR in [13]. Despite their small dimensions, these designs exhibit lower EMR values. Additionally, they display fewer resonance peaks compared to the NH-SRR metamaterial, three resonances shown in [30] and only one the case in [13]. On the other hand, while the designs reported in [27], Greek, and [28] achieve excellent EMR values, even comparable to our work in the case of [31], they feature only tri-band resonance modes within their operating frequency ranges, which is four fewer than the resonance peaks observed in our structure. Another crucial point of comparison is the number of resonance peaks. Most existing designs typically exhibit fewer resonance peaks, ranging from just one in [13] and [32] to four, as seen in [29], [31], and others. In summary, the NH-SRR based metamaterial design proposed in this article stands out thanks to its compact size, relatively high EMR, and, most notably, its seven resonance peaks, which offers a more complex and potentially versatile frequency response. The ability of the NH-SRR based metamaterial to achieve multiple resonances across these bands not only supports wideband performance but also improves gain and reduces radiation loss, enhancing the overall efficiency and effectiveness of the antenna systems in these applications..

Table 6. *The comparison of proposed work with some published researches in term of effective performance.*

Reference	Shape	Substrate	Size ($mm \times mm$)	Resonance Frequency (GHz)	Cover band	Max EMR
[13]	Circle-shaped SRR	Rogers RT5880	9×9	7.44	C	7.33
[17]	Interlinked SRR	FR4	10×10	3.95, 9.57, 13.68	L, S, X	8.03
[19]	Square shaped SRR	FR-4	9.5×9.5	2.5, 4.9 and 6	S and C	9.96
[21]	Square Shaped SRR	FR-4	14.5×14.5	4.3 and 9.1	C and X	6.2
[27]	Z-Shaped Resonator	FR-4	10×10	3.29, 7.62, 10.92, and 12.57	S, C, X and Ku	9.12
[28]	Complementary double H-shaped SRR	FR-4	9×9	3.1, 10.1, 11.8 and 12.44	S, C, X and Ku	10.75
[29]	H-shaped	FR-4	30×30	2.74, 7.122, 10.855 and 14.337	S, C, X and Ku	3.65
[30]	Combination of circular and square SRR	FR-4	8×8	5.80 and 16.61	C and Ku	6.47
[31]	Greek-key pattern	Rogers RO3010	10×10	2.4; 3.5 and 4	S and C	12.5
[32]	V-shaped conductive strips	Rogers RO4350B	5×5	8.1	X	10.0
[33]	Z-shaped	Epoxy	6×6	6.4	C	7.81
proposed	Nested Hexagonal-SRR	Rogers RO4350B	11×10	2.37; 3.92; 5.4; 7.71, 8.58; 9.73 and 10.94	S, C and X	12.66

3.5. Gain Enhancement of LPDA Antenna Using an Array Cover of the Proposed ENG Metamaterial

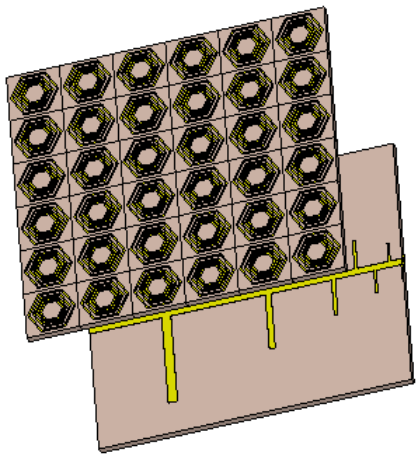

Figure 10. *LPDA antenna with metamaterial cover.*

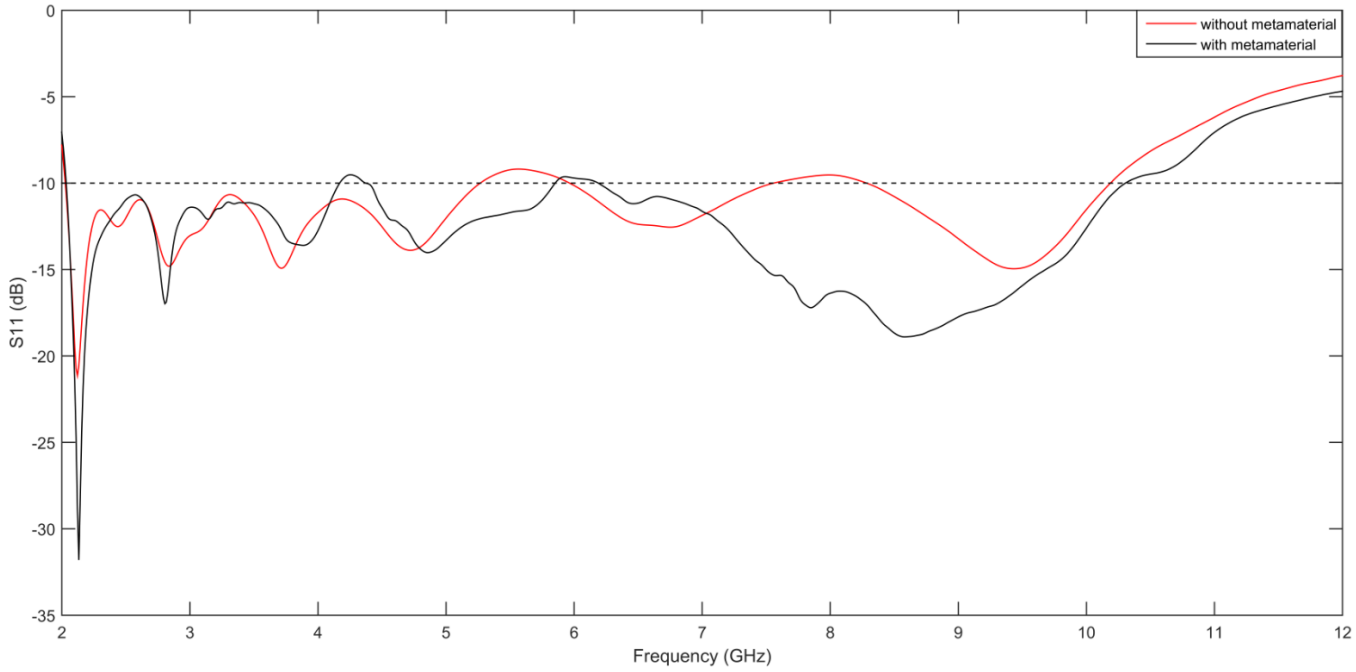

Figure 11. *The reflection coefficient of the LPDA antenna with/without metamaterial.*

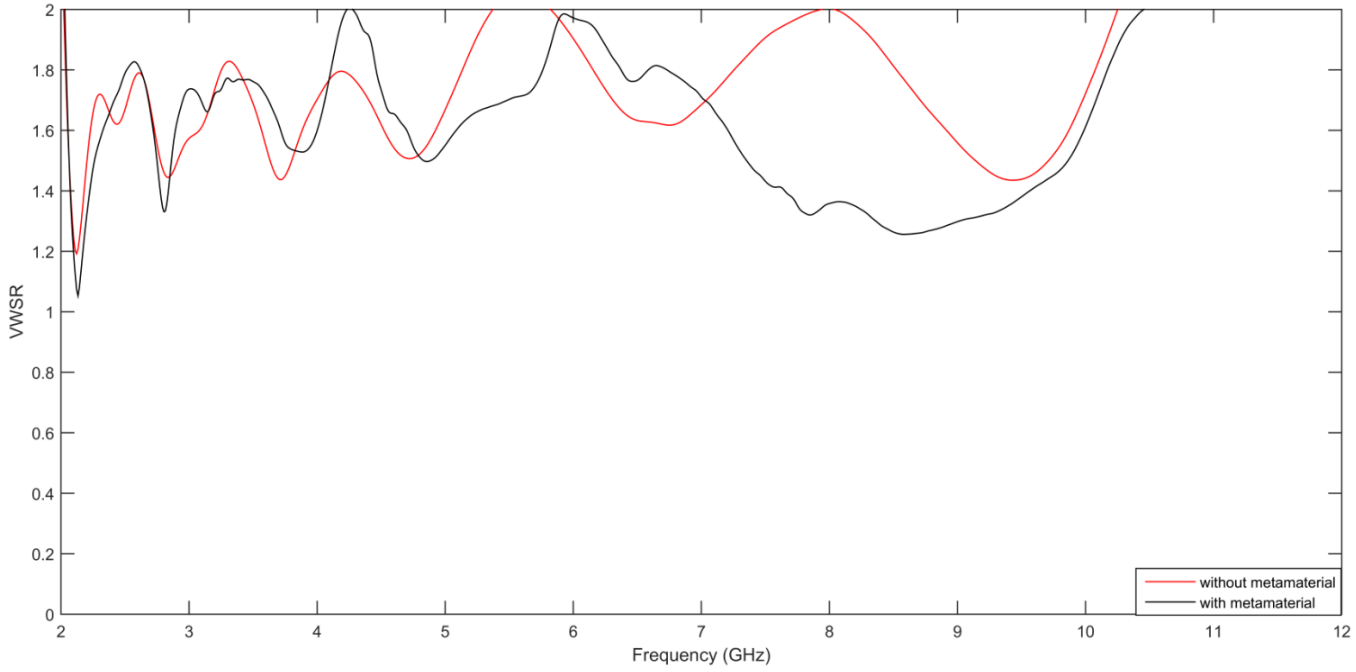

Figure 12. *VSWR of the LPDA antenna with/without metamaterial.*

As previously discussed, the proposed multiband NH-SRR-based metamaterial features a negative permittivity response and near-zero permeability properties. These characteristics make the reported metamaterial an excellent candidate for addressing gain limitations in microwave antenna devices, where radiation efficiency is critical for performance. To this end, an LPDA antenna was designed to operate across the S, C, and X-bands and simulated using the transient solver in CST Microwave Studio. The antenna measures $65\ mm \times 54.4\ mm$ and consists of 10 metallic dipole arms connected via a 50 Ω microstrip feeding line, printed on both side of 1.6 mm thick FR-4 substrate with dielectric constant $\epsilon_r = 4.3$ and tangent loss $tan\delta = 0.02$. A metamaterial superstrate, composed of a 6×6 unit cell array is applied 45 mm above the LPDA antenna as depicted in Figure 10. The obtained antenna simulation outcomes in term of refection coefficient are presented in

Figure 11, where it can be observed that the antenna achieved a -10 dB return loss. It is noticeable that the metamaterial-integrated antenna provides the same bandwidth but achieves a more consistent and lower s11 parameter compared to the antenna without the metamaterial, particularly at resonance frequencies. The Voltage Standing Wave Ratio (VSWR) results, shown in Figure 12, indicate that the metamaterial-integrated antenna achieves lower radiations losses compared to the antenna without the metamaterial. The parameter consistently not only remains below 2 across much of the operating frequency band but as close as 1, which leads to better power transfer between the antenna and the transmission line when the metamaterial superstrate is applied. In term of gain, the metamaterial-modified antenna exhibited substantial multiband improvements especially where the negative electric permittivity response located, as evident in Figure 13. In the lower and mid-frequencies (S and C-bands), the metamaterial-enhanced antenna consistently outperforms the standard configuration, with a notable gain improvement of 0.91 dB and 0.87 dB at 3.92 GHz and 5.4 GHz, respectively. The enhancement becomes more pronounced at higher frequencies, where the gain improvement reaches approximately 1.01 dB at 7.71 GHz, 1.50 dB at 8.58 GHz, 1.77 dB at 9.73 GHz, and 1.21 dB at 10.94 GHz (X-band). The performance enhancements can be attributed to the negative permittivity feature that allows the metamaterial cover to redirect the reflected beams and confine electromagnetic energy within the metallic elements of the antenna as meticulously explained in [10–12]. As a result, the concentration of the redirected electric field decreases radiation losses and prevents inefficient energy dispersion, significantly increasing the electromagnetic field intensity in the horizontal plane of the LPDA antenna and enhancing its gain. In summary, by manipulating the electromagnetic environment around the antenna, the proposed ENG metamaterial superstrate focuses radiation patterns, reduces signal loss, and boosts horizontal gain. These findings confirm that the proposed metamaterial offers a promising solution for improving satellite, radar, and wireless communication systems, where high gain and broad frequency coverage are essential.

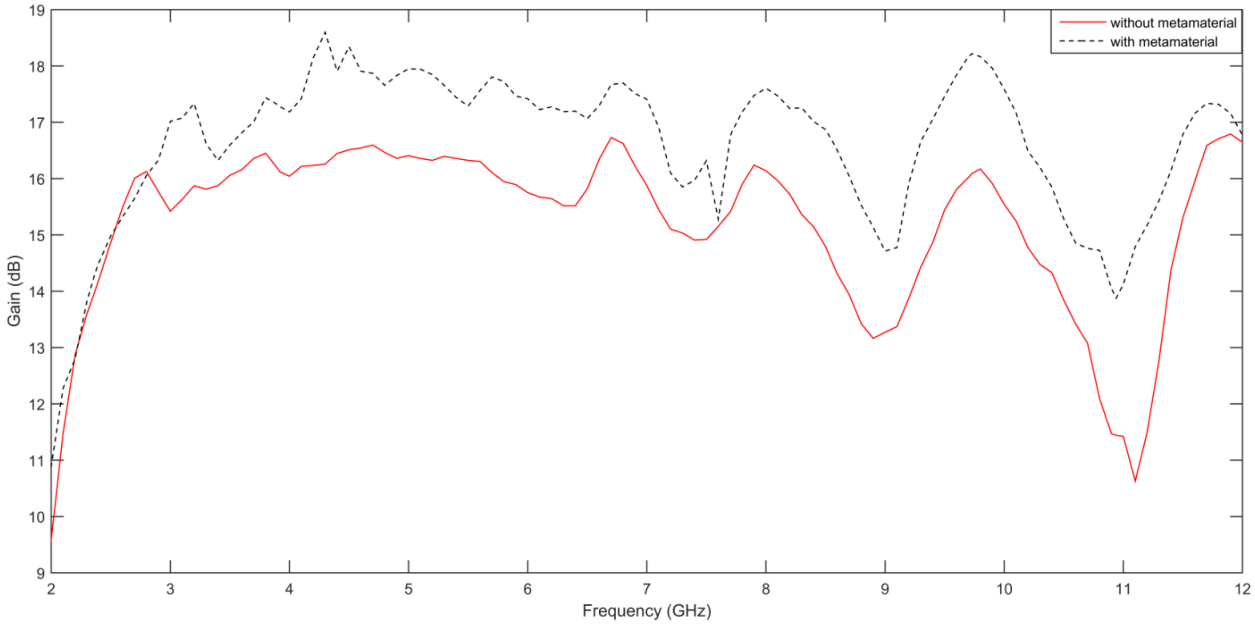

Figure 13. *The gain of the LPDA antenna with/without metamaterial.*

4. Conclusion

In this report, the effective propagation characteristics of four distinct hexagonal-shaped SRR-based metamaterial structures designed for triple-band operation with wide bandwidth were examined over the frequency range of 2-12 GHz. The introduced metamaterial sample exhibited seven distinct resonance frequencies at 2.37, 3.92, 5.4, 7.71, 8.58, 9.73, and 10.94 GHz. The analysis revealed that the metamaterial in question possesses unique electromagnetic properties, including negative permittivity and near-zero permeability, suitable for multiband operations. The EMR of the designed structure is 12.66, indicating that the design is compact and holds potential applications in the microwave region, effectively covering all three frequency bands. CST Microwave Studio, COMSOL, and HFSS were employed for the design, simulation, and optimization of the metamaterial's performance, with the results cross-verified by comparing outcomes across these simulation tools. With all features which suggest that the reported nested hexagonal SRR-shaped metamaterial can be a prominent solution for enhancing emerging satellite communications and radar applications. Its small size, multiband resonance, high EMR, and wideband characteristics make it a valuable component for improving

multiband antennas. Further investigation into LPDA antenna revealed that the integration of the metamaterial significantly improved the antenna's performance in terms of gain and efficiency, thereby validating the aim of this research.

Abbreviations

CST	Computer Simulation Technology
EMR	Effective Medium Ratio
ENG	Epsilon-Negative
FIT	Finite Integration Technique
FR-4	Flame Retardant Substrate
HFSS	High-Frequency Structure Simulator
LPDA	Log Periodic Dipole Array
MATLAB	Matrix Laboratory
NH-SRR	Nested Hexagonal Split Ring Resonator
NZI	Near-Zero Index
SRR	Split Ring Resonator
VSWR	Voltage Standing Wave Ratio

ORCID

0009-0007-5449-7947 (Hassan Belaid)

Author Contributions

The author confirms being the sole contributor to this work and has approved it for publication. The author was responsible for the conception and design of the study, data collection, analysis and interpretation, manuscript drafting, and final approval of the version to be published.

Conflicts of Interest

The author declares no conflict of interest.

References

[1] D. R. Smith, J. B. Pendry, and M. C. K. Wiltshire, Metamaterials and negative refractive index, *Science*, 2004, vol. 305, pp. 788-792, https://doi.org/10.1126/science.1096796

[2] Z. Li, S. Chen, Y. Zhang, C. Tong, X. Guo, J. Shen, and C. Li, Terahertz band range adjustable hyperbolic metamaterial refractive index sensor, *Results in Physics*, 2023, vol. 49, p. 106477, https://doi.org/10.1016/j.rinp.2023.106477

[3] D. Schurig, J. J. Mock, B. J. Justice, S. A. Cummer, J. B. Pendry, A. F. Starr, and D. R. Smith, Metamaterial electromagnetic cloak at microwave frequencies, *Science*, 2006, vol. 314, no. 5801, pp. 977-980, https://doi.org/10.1126/science.1133628

[4] H. Chen and M. Chen, Flipping photons backward: Reversed Cherenkov radiation, *Materials Today*, 2011, vol. 14, no. 1-2, pp. 34-41, https://doi.org/10.1016/S1369-7021(11)70020-7

[5] D. Ziemkiewicz and S. Zieliska-Raczyska, Complex Doppler effect in left-handed metamaterials, *Journal of the Optical Society of America B*, 2015, vol. 32, pp. 363-369, https://doi.org/10.1364/JOSAB.32.000363

[6] J. B. Pendry, A. J. Holden, W. J. Stewart, and I. Youngs, Extremely low frequency plasmons in metallic mesostructures, *Physical Review Letters*, 1996, vol. 76, no. 25, pp. 4773-4776, https://doi.org/10.1103/PhysRevLett.76.4773

[7] Jan Krzysztofik W, Nghia Cao T. Metamaterials in Application to Improve Antenna Parameters. 2019. https://doi.org/10.5772/intechopen.80636

[8] Xu, Wendao; Xie, Lijuan; Ying, Yibin, Mechanisms and applications of terahertz metamaterial sensing: a review, *Nanoscale*, 2017, vol.9, pp.13864-13878, https://doi.org/10.1039/C7NR03824K

[9] Tian, Shuncheng, Zhang, Xuanming, Wang, Xin, Han, Jiaqi and Li, Long. Recent advances in metamaterials for simultaneous wireless information and power transmission, *Nanophotonics*, 2022, vol. 11, no. 9, pp. 1697-1723. https://doi.org/10.1515/nanoph-2021-0657

[10] M. R. Islam et al., Square enclosed circle split ring resonator enabled epsilon negative (ENG) near zero index (NZI) metamaterial for gain enhancement of multiband satellite and radar antenna applications, *Results in Physics*, 2020, vol. 19, p. 103556, https://doi.org/10.1016/j.rinp.2020.103556

[11] M. Moniruzzaman, M. T. Islam, N. Misran, et al., Inductively tuned modified split ring resonator based quad band epsilon negative (ENG) with near zero index (NZI) metamaterial for multiband antenna performance enhancement, *Scientific Reports*, 2021, vol. 11, p. 11950, https://doi.org/10.1038/s41598-021-91432-8

[12] M., S. M., V., B. G., and S. M., U. Gain enhancement of patch antenna integrated with metamaterial inspired superstrate, *Journal of Electrical Systems and Information Technology*, 2018, vol. 5, no. 3, pp. 263-270, https://doi.org/10.1016/j.jesit.2018.04.002

[13] M. Moniruzzaman, M. T. Islam, I. Hossain, et al., Symmetric resonator based tunable epsilon negative near zero index metamaterial with high effective medium ratio for multiband wireless applications, *Scientific Reports*, 2021, vol. 11, p. 21842, https://doi.org/10.1038/s41598-021-01266-7

[14] Moniruzzaman, M.; Islam, M. T.; Islam, M. R.; Misran, N.; Samsuzzaman, M., Coupled ring split resonator (CR-SRR) based epsilon negative metamaterial for multiband wireless communications with high effective medium ratio, *Results in Physics*, 2020, vol. 18, p. 103248, https://doi.org/10.1016/j.rinp.2020.103248

[15] B. Ajewole, P. Kumar, and T. I. Afullo, I-Shaped Metamaterial Using SRR for Multi-Band Wireless Communication, *Crystals*, 2022, vol. 12, no. 559, https://doi.org/10.3390/cryst12040559

[16] A. M. Lima, N. H. O. Cunha, J. P. D. Silva, Effect of metamaterial cells array on a microstrip patch antenna design, *Journal of Microwaves, Opto-electronics and Electromagnetic Applications*, 2020, vol. 19, pp. 327-342, https://doi.org/10.1590/2179-10742020v19i3886

[17] Moniruzzaman, Md Islam, Mohammad Islam, Md Tarikul Rmili, Hatem Samsuzzaman, Md. Cross Coupled Interlinked Split Ring Resonator Based Epsilon Negative Metamaterial with High Effective Medium Ratio for Multiband Satellite and Radar Communications. *Results in Physics*. 2020. vol.18, pp 103296. https://doi.org/10.1016/j.rinp.2020.103296

[18] Ankit, M. N. Baitha, K. Kishor, R. K. Sinha, Quadrupole mode plasmon resonance enabled dual-band metamaterial for refractive index sensing application, *Journal of Applied Physics*, 2024, vol. 136, no. 2, p. 023104, https://doi.org/10.1063/5.0201422

[19] M. L. Hakim, M. T. Islam, T. Alam, S. K. Abdul Rahim, B. Bais, M. S. Islam, M. S. Soliman, Triple-Band Square Split-Ring Resonator Metamaterial Absorber Design with High Effective Medium Ratio for 5G Sub-6 GHz Applications, *Nanomaterials*, 2023, vol. 13, no. 2, p. 222, https://doi.org/10.3390/nano13020222

[20] T. Alam, M. T. Islam, M. L. Hakim, K. H. Alharbi, M. S. J. Singh, M. M. Sheikh, R. W. Aldhaheri, M. S. Islam, M. S. Soliman, Metamaterial Based Ku-Band Antenna for Low Earth Orbit Nanosatellite Payload System, *Nanomaterials*, 2023, vol. 13, no. 2, p. 228, https://doi.org/10.3390/nano13020228

[21] S. Hossen, A. Alqahtani, I. Hossain, M. T. Islam, M. Moniruzzaman, M. Samsuzzaman, Gap coupled symmetric square split ring high EMR resonator based metamaterial for S-, C-, and X-bands wireless applications: Simulation and experiment, *Optical Materials*, 2023, vol. 145, p. 114389, https://doi.org/10.1016/j.optmat.2023.114389

[22] X. Chen, T. M. Grzegorczyk, B.-I. Wu, J. Pacheco, J. A. Kong, Robust method to retrieve the constitutive effective parameters of metamaterials, *Physical Review E*, vol. 70, p. 016608, 2004, https://doi.org/10.1103/PhysRevE.70.016608

[23] A. Castani? J. Mercier, S. Félix, A. Maurel, Generalized method for retrieving effective parameters of anisotropic metamaterials, *Optics Express*, 2014, vol. 22, no. 24, pp. 649-661, https://doi.org/10.1364/OE.22.029937

[24] D. R. Smith, D. C. Vier, C. M. Soukoulis, Electromagnetic parameter retrieval from inhomogeneous metamaterials, *Physical Review E*, 2005, vol. 71, no. 3, p. 036617, https://doi.org/10.1103/PhysRevE.71.036617

[25] T. J. Cui, D. R. Smith, and R. Liu, *Metamaterials: Theory, Design, and Applications*, 2010. https://doi.org/10.1007/978-1-4419-0573-4

[26] T. Koschny, M. Kafesaki, E. N. Economou, and C. M. Soukoulis, Effective medium theory of left-handed materials, *Physical Review Letters*, 2004, vol. 93, no. 10, no. 107402, https://doi.org/10.1103/PhysRevLett.93.107402

[27] Hasan Md and Faruque M. R. I., Left-handed metamaterial using Z-shaped SRR for multiband application by azimuthal angular rotations, *Materials Research Express*, vol. 4, no. 4, 2017, https://doi.org/10.1088/2053-1591/aa6a7e

[28] A. M. Siddiky, M. R. I. Faruque, M. T. Islam, Double H-shaped complementary split ring resonator with different orientations for quad-band satellite applications, *Results in Physics*, 2020, vol. 19, p. 103427, https://doi.org/10.1016/j.rinp.2020.103427

[29] S. S. Islam, M. R. I. Faruque, and M. T. Islam, The design and analysis of a novel H-shaped metamaterial for multi-band microwave applications, *Materials*, 2014, vol. 7, pp. 4994-5011, https://doi.org/10.3390/ma7074994

[30] T. Ramachandran, M. R. I. Faruque, M. T. Islam, A dual band left-handed metamaterial enabled design for satellite applications, *Results in Physics*, 2020, vol. 16, p. 102942, https://doi.org/10.1016/j.rinp.2020.102942

[31] B. Zarghooni, A. Dadgarpour, T. A. Denidni, Greek-key pattern as a miniaturized multiband metamaterial unit-cell, *IEEE Antennas and Wireless Propagation Letters*, 2015, vol. 14, pp. 1254-1257, https://doi.org/10.1109/LAWP.2015.2400820

[32] E. Ekmekci and G. T. Sayan, Investigation of effective permittivity and permeability for a novel V-shaped metamaterial using S-parameters, in *Proceedings of the 5th International Conference on Electrical and Electronics Engineering, Bursa, Turkey*, 2007.

[33] A. Dhouibi, S. N. Burokur, A. Lustrac, and A. Priou, Study and analysis of an electric Z-shaped meta-atom, *Advances in Electromagnetics*, 2012, vol. 1, pp. 64-70, https://doi.org/10.7716/aem.v1i2.82